J Mater Sci (2008) 43:2978–2989
DOI 10.1007/s10853-007-2130-8

INTERFACE SCIENCE

Effect of platinum on the oxide-to-metal adhesion in thermal barrier coating systems

H. M. Tawancy · A. UI-Hamid · N. M. Abbas · M. O. Aboelfotoh

Received: 13 June 2007 / Accepted: 27 August 2007 / Published online: 18 October 2007

Abstract An investigation was conducted to determine the role of Pt in a thermal barrier coating system deposited on a nickel-base superalloy. Three coating systems were included in the study using a layer of yttria-stabilized zirconia as a model top coat, and simple aluminide, Pt-aluminide, and Pt bond coats. Thermal exposure tests at 1,150 °C with a 24-h cycling period to room temperature were used to compare the coating performance. Additional exposure tests at 1,000, 1,050, and 1,100 °C were conducted to study the kinetics of interdiffusion. Microstructural features were characterized by scanning electron microscopy and transmission electron microscopy combined with energy dispersive X-ray spectroscopy as well as X-ray diffraction. Wavelength dispersive spectroscopy was also used to qualitatively distinguish among various refractory transition metals. Particular emphasis was placed upon: (i) thermal stability of the bond coats, (ii) thickening rate of the thermally grown oxide, and (iii) failure mechanism of the coating. Experimental results indicated that Pt acts as a "cleanser" of the oxide-bond coat interface by decelerating the kinetics of interdiffusion between the bond coat and superalloy substrate. This was found to promote selective oxidation of Al resulting in a purer Al_2O_3 scale of a slower growth rate increasing its effectiveness as "glue" holding the ceramic top coat to the underlying metallic substrate. However, the exact effect of Pt was found to be a function of the state of its presence within the outermost coating layer. Among the bond coats included in the study, a surface layer of Pt-rich γ'-phase ($L1_2$ superlattice) was found to provide longer coating life in comparison with a mixture of $PtAl_2$ and β-phase.

H. M. Tawancy (✉) · A. UI-Hamid · N. M. Abbas
Center for Engineering Research, King Fahd University of Petroleum & Minerals, Dhahran 31261, Saudi Arabia
e-mail: tawancy@kfupm.edu.sa

M. O. Aboelfotoh
Department of Materials Science and Engineering, North Carolina State University, Raleigh, NC 27695, USA

Introduction

The use of thermal barrier coatings (TBC) as surface protection systems for turbine blades is considered one of the most viable means for increasing the turbine entry temperature [1–4]. Current technology involves the use of a multi-layer coating consisting of: (i) an outer ceramic layer usually zirconia (ZrO_2) stabilized by 8–10 wt.% yttria (Y_2O_3) and about 200–250 μm in thickness (top coat), and (ii) an inner layer of a metallic coating applied to the turbine blade alloy and varying in thickness from 50 to 150 μm (bond coat). Various modifications of bond coats are essentially based upon the conventional metallic coatings, which are of two types: (i) diffusion coatings applied by electroplating followed by a diffusion heat treatment such as aluminides and their modifications, and (ii) non-diffusion or overlays usually applied by low-pressure plasma spraying such as overlays (MCrAlY-type where M is Ni, Co, or Ni + Co). It is the primary function of the bond coat to develop a thin tenacious layer of aluminum oxide (Al_2O_3) about 1 μm in thickness to act as "glue" holding the top coat to the substrate. This is achieved by a pre-oxidation heat treatment prior to application of the topcoat [5]. Another important function of the bond coat is to provide an additional resistance to oxidation and hot corrosion. Typically, the topcoat is applied by the technique of electron-beam physical vapor deposition (EBPVD). Although low-pressure plasma spraying can also be used,

however, it typically produces coatings of high surface roughness, high porosity, low thermal stability, and relatively poor resistance to hot-gas corrosion. Upon exposure at elevated temperatures, the thickness of initial oxide layer increases at a rate determined by the structure and properties of the bond coat for a given superalloy substrate. The newly formed oxide is commonly referred to as thermally grown oxide. Several studies had demonstrated that the adhesion between the thermally grown oxide and bond coat plays a dominant role in determining the life of the TBC system. [1, 6–15]. However, another contributing factor was shown to be surface rumpling of the bond coat [16–18], which is known to occur in thin-film materials [19].

Most of the interest in extending the life of TBC systems particularly under thermal cycling conditions is focused on developing bond coats with better oxidation properties. Earlier studies had demonstrated that the addition of platinum (Pt) to simple aluminide coatings could significantly improve the protective nature of the surface layer of Al_2O_3 scale developed during exposure at elevated temperatures [20–23]. Therefore, this study was undertaken to determine the effect of Pt on the performance of three TBC systems using the same top coat (yttria-stabilized zirconia) and alloy substrate. Two Pt-modified bond coats were included in the study. For comparative purposes, a simple aluminide coating free of Pt was also included.

Experimental procedure

The alloy substrate used in this study was in single crystal form (rods about 8 mm in diameter). Its nominal chemical composition is listed in Table 1. All coatings used in this study were of commercial grade and applied by standard industry practices. A simple aluminide coating free of Pt (nominal Al content of 25 wt.%) was applied by the pack cementation process [24, 25]. Rods of the alloys included in the study were grit blasted and then placed in an airtight retort containing a powder mixture of aluminum and a halide activator. The assembly is heated for 4 h at 1,000 °C to promote diffusion. Platinum aluminizing to produce nominal Pt and Al contents of 55 and 25 wt.% respectively was carried out by first electroplating a 6–8-μm thick layer of Pt on the alloy surface followed by diffusion and aluminizing treatments [26]. All diffusion heat treatments were carried out for 4 h at 1,150 °C. Both the aluminide and Pt-aluminide coatings had a nominal thickness of about 40-μm in the annealed condition. A Pt bond coat was developed by electroplating about 10-μm thick layer of Pt on the alloy surface followed by a diffusion heat treatment to develop a coating layer about 40 μm in thickness. For all three bond coats, a layer of the ceramic top coat (ZrO_2 + 8 wt.% Y_2O_3) about 250 μm in thickness was applied by the EBPVD technique. Rod samples were oriented at about 30° to the evaporation source and rotated about their longitudinal axis to ensure a uniform coating thickness. The coating chamber was evacuated to about 2 Pa. All samples were preheated to 970 °C. Deposition was carried out at a rate of about 1 μm/s. Coating performance was evaluated by thermal exposure tests at 1,150 °C in still air with a 24-h cycling period to room temperature until failure occurred as indicated by spallation of the topcoat. Samples about 8 mm in diameter and 5 mm in thickness were placed in crucibles and furnace-heated to 1,150 °C under normal atmospheric conditions. Every 24 h, the crucibles were removed from the furnace, cooled to room temperature, and then replaced in the furnace. Failure was detected by the first observation of macroscopic separation of the topcoat. Also, the same test was used to determine the thermal stability characteristics of the bond coats. Additional thermal exposure tests without cycling to room temperature were carried out at 1,000 and 1,050 °C, and 1,100 °C for up to 1,000 h to study the kinetics of interdiffusion between the bond coat and alloy substrate. Various techniques including scanning electron microscopy, transmission electron microscopy, microchemical analysis, and X-ray diffraction were used to characterize the microstructure. Samples for scanning electron microscopy and microchemical analysis were examined in the as-polished condition. A JEOL 5800LV SEM was used at 20 kV. Quantification of the energy dispersive spectral data was carried out by a software based upon the standard method with relative peak intensities using internal standards. Qualitative wavelength dispersive spectroscopy to distinguish refractory transition metals particularly W, Ta, and Re was carried out in a JEOL 733 superprobe at 20 kV. To observe the oxide phase by transmission electron microscopy parallel to the plane of oxidation, thin foils were prepared by a standard technique consisting of electropolishing and ion beam thinning as described in reference [27]. First, oxidized specimens were electropolished on the metal side approaching the oxide-metal interface until perforation occurred. Electropolishing was carried out in a solution of 30% nitric acid in methanol maintained at about –20 °C. This was followed by ion beam thinning at 5 kV. Fine particles within the coatings such as $PtAl_2$ in the Pt-aluminide were analyzed by the technique of microdiffraction using a probe diameter of 1 nm. All foils were examined at 200 KV using a JEOL 2000EX analytical electron microscope.

Table 1 Nominal chemical composition of the alloy substrate (wt.%)

Ni	Co	Cr	Ta	W	Al	Re	Ti	Mo	Hf
Bal.	9.5	6.2	6.5	6.5	5.5	2.9	1.0	0.8	0.1

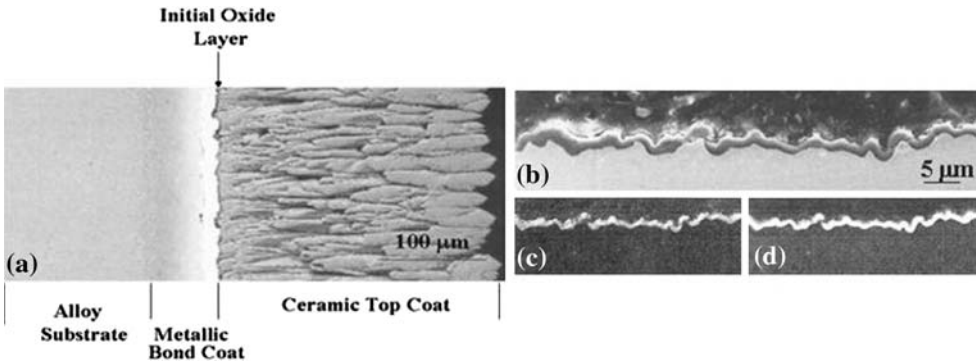

Fig. 1 An example derived from the system containing the Pt-aluminide bond coat to illustrate the initial oxide layer at the surface of the bond coat in the heat-treated condition. (**a**) Backscattered electron image showing the microstructure along a cross section of the coating system and into the alloy substrate. (**b**) Backscattered electron image illustrating the oxide layer. (**c**) and (**d**) are corresponding X-ray mapping images of O and Al respectively

Results and discussion

Coating performance

A typical microstructure of a thermal barrier coating system in the heat-treated condition along a cross section of the coating and into the alloy substrate is shown in the backscattered electron image of Fig. 1. Regardless of the type of bond coat, the average thickness of the initial layer of Al_2O_3 was about 1 μm.

Figure 2 shows the average lives of the three coating systems included in the study as determined from thermal exposure tests at 1,150 °C with a 24-h cycling period to room temperature. Failure was indicated by the onset of spallation of the top coat. Qualitatively, the behavior of the initial oxide layer during thermal exposure at 1,150 °C was similar for all bond coats included in the study. The oxide layer continued to grow until decohesion with the bond coat occurred leading to spallation of the top coat. An example derived from the Pt-aluminide bond coat is given in Fig. 3.

It is evident from the above results that Pt-containing bond coats provided a better performance, however, the exact effect of Pt appeared to be dependent upon its state of presence in the bond coat. Also, Pt appeared to decelerate the kinetics of the process leading to loss of adhesion between the oxide layer and underlying bond coat. This behavior could be understood in terms of the differences in initial microstructural features of the bond coats and the changes which occur during subsequent exposure at elevated temperatures (Fig. 3).

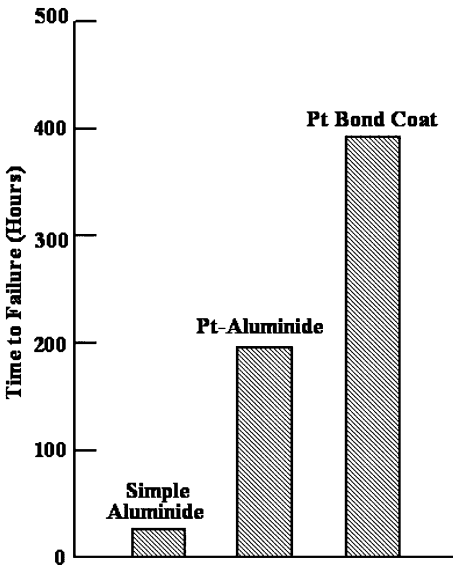

Fig. 2 Comparative performance of the thermal barrier coating system as a function of the bond coat

Initial microstructures of the bond coats

Typical microstructural features of the simple aluminide coating in the heat-treated condition are summarized in Fig. 4. As can be seen from Fig. 4a, the coating consisted of an outer fine-grained layer followed by a coarse-grained layer, and an inner interdiffusion zone of a columnar morphology typical of a coating produced by inward diffusion of Al [28, 29]. Secondary precipitates exhibiting white contrast at the grain boundaries of the b-phase in the coating layer were found to be particles of the Ni–Cr–W σ-phase. Some of the finer particles were of α-Cr. The lamellar phase within the interdiffusion zone exhibiting white contrast was found to be of the Ni–Cr–W σ-phase. As expected, the X-ray diffraction pattern of Fig. 4b shows that the outer coating layer consisted of β-NiAl (B2-type superlattice), however, weaker reflections characteristic of α-Cr (bcc structure) could also be detected. Figure 4c shows the elemental composition of the β-phase as determined by energy dispersive spectroscopy indicating that it

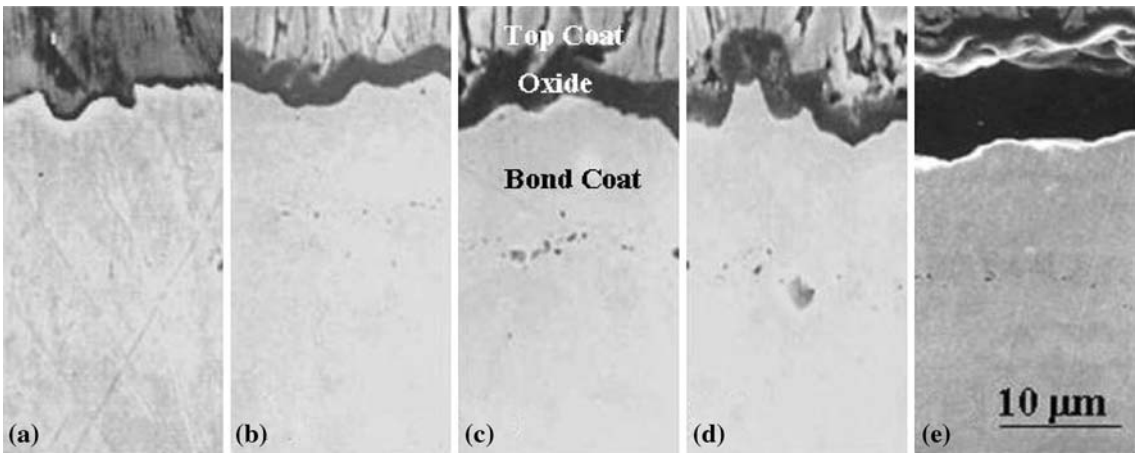

Fig. 3 An example derived from the Pt-aluminide bond coat to illustrate the effect of exposure time at 1,150 °C on the oxide thickness and eventually decohesion between the oxide and bond coat (secondary electron images). (**a**) Heat-treated condition. (**b**) 24 h of exposure. (**c**) 72 h of exposure. (**d**) 120 h of exposure. (**e**) 168 h of exposure (localized decohesion between the oxide and bond coat; complete spallation of the top coat occurred after 192 h of exposure)

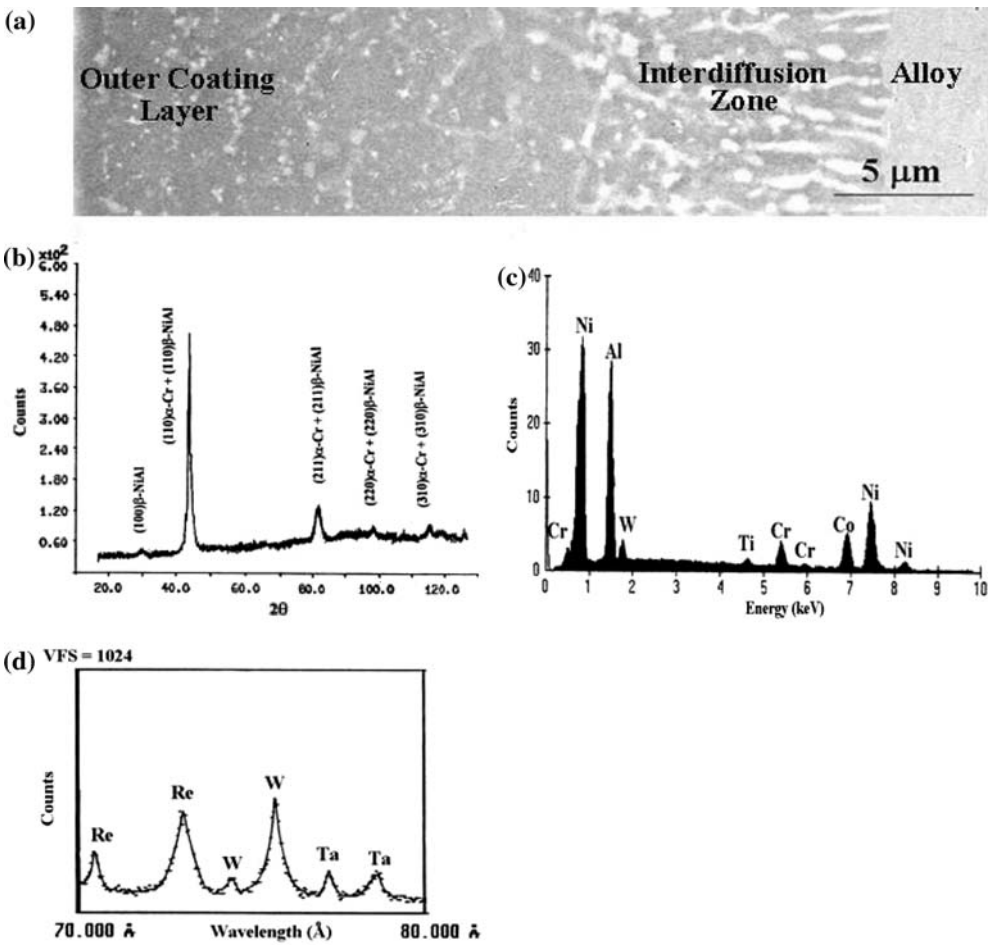

Fig. 4 Characteristic microstructural features of the aluminide bond coat in the heat-treated condition. (**a**) Backscattered electron image along a cross section of the bond coat. (**b**) An X-ray diffraction pattern derived from the surface. (**c**) An energy dispersive X-ray spectrum showing the elemental composition of the outermost coating layer. (**d**) A wavelength dispersive spectrum showing the co-existence of Re, W, and Ta in the outermost coating layer

contained other elements in solid-solution particularly Co, Ti, and Cr. Since the differences between the characteristic energies of W, Ta, and Re are less than the spectral resolution, it was not possible to distinguish these elements by energy dispersive spectroscopy. However, wavelength dispersive spectroscopy showed that the peak labeled W in Fig. 4c was due to W, Ta, and Re as shown in Fig. 4d. The presence of α-Cr within the outer coating layer was further confirmed by transmission electron microscopy as illustrated in Fig. 5. It is known that the presence of refractory transition metals near the surface degrade the protective nature of Al_2O_3 scale [30]. Also, the presence of α-Cr is known to have detrimental effects on oxidation resistance [31, 32]. As shown below both of these effects were minimized in the Pt-aluminide bond coat.

Figure 6 shows typical microstructural features of the Pt-aluminide bond coat in the heat-treated condition. Similar to the simple aluminide coating, Fig. 6a shows that the Pt-aluminide bond coat consisted of three distinct layers. However, the outer coating layer consisted of a mixture of β-NiAl and $PtAl_2$ (cubic: CaF_2-type structure) as shown in the X-ray diffraction pattern of Fig. 6b. Also, there was no evidence for the presence of α-Cr precipitates in the outer coating layer. Furthermore, the energy dispersive X-ray spectrum of Fig. 6c indicates that the outer coating layer was relatively free of refractory transition metals in contrast with the case of the simple aluminide bond coat. An example is given in Fig. 7 to illustrate the microstructure of $PtAl_2$ as revealed by transmission electron microscopy. As can be seen in the dark-field image of Fig. 7a, $PtAl_2$ was present as a fine dispersion within a matrix of β-phase exhibiting a dark contrast. A microdiffraction pattern in ⟨001⟩ orientation is shown in the inset. The corresponding elemental composition is shown in the energy dispersive spectrum of Fig. 7b. Also, microchemical analysis showed that the β-phase in the outer coating layer contained Pt, which could replace for both Ni and Al. In contrast, the inner coating layer consisting of β-phase relatively free of Pt was found to contain refractory transition metals similar to the case of the outer coating layer of the simple aluminide. Also, this layer contained precipitates of α-Cr. Therefore, it could be concluded that a dispersion of $PtAl_2$ in a matrix of Pt-containing β-phase provided higher diffusional stability minimizing the outward diffusional transport of refractory transition metals during coating formation. Also, these results suggested that the outer coating layer of the Pt-aluminide coating had a higher solubility for Cr reducing the tendency to precipitate α-Cr.

In the heat-treated condition, the Pt bond coat consisted of an outer layer of a dense compact γ'-phase ($L1_2$ superlattice) followed by a columnar layer of γ'-phase containing islands of γ-phase (solid-solution), and an alloy-depleted zone as shown in the backscattered image of Fig. 8a and X-ray diffraction pattern of Fig. 8b. Typical compositions

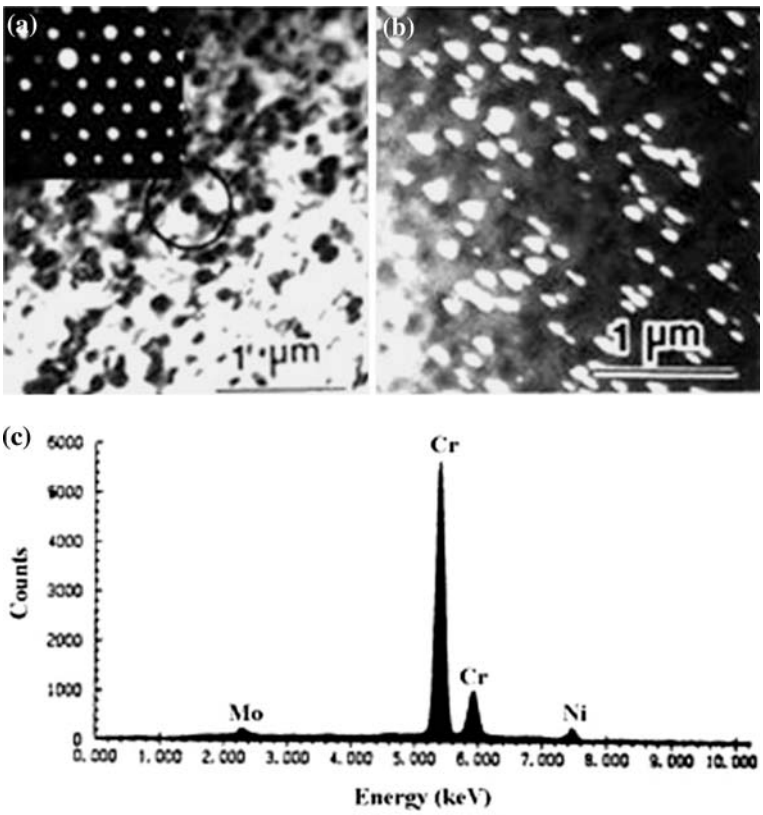

Fig. 5 Identification of α-Cr precipitates in the outermost coating layer of the aluminide bond coat. (**a**) Bright-field TEM image, the inset is a microdiffraction pattern derived from a precipitate particle in ⟨111⟩ orientation. (**b**) Corresponding dark-field image. (**c**) An energy dispersive spectrum showing a typical elemental composition of the precipitates

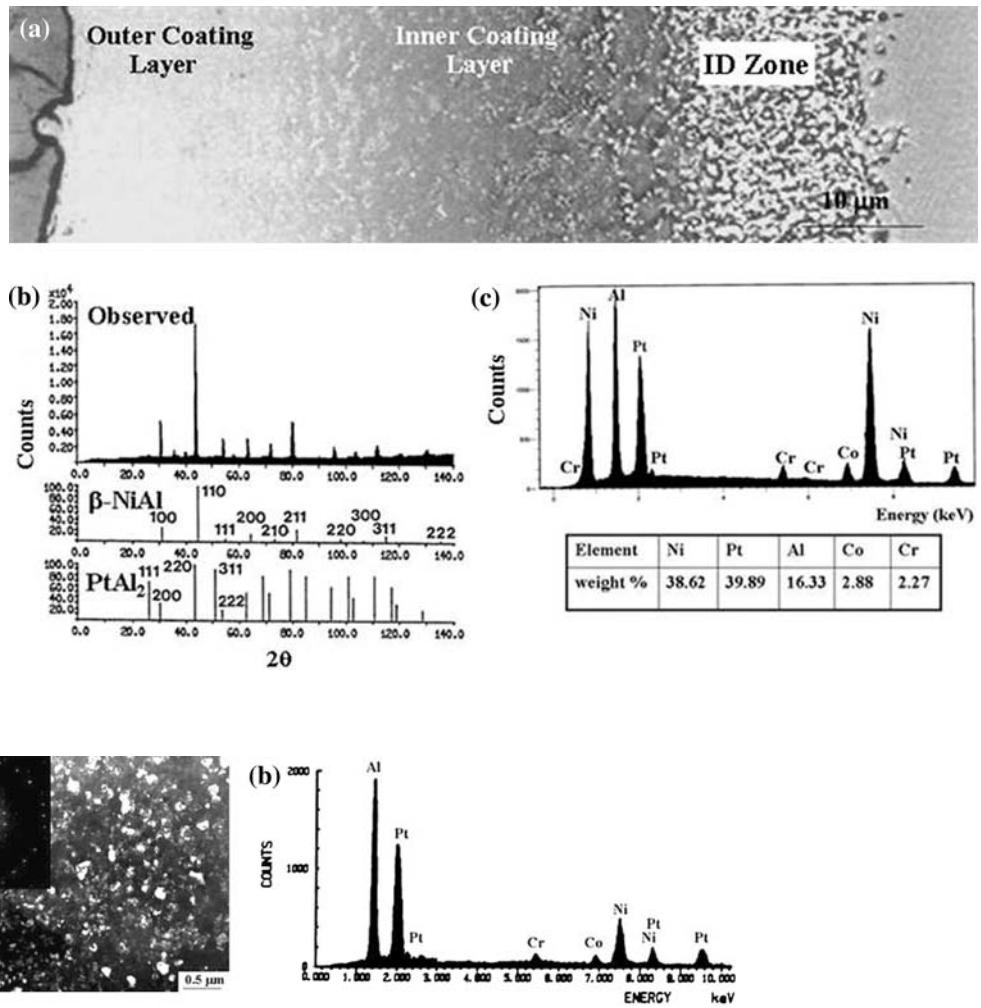

Fig. 6 Characteristic microstructural features of the Pt-aluminide bond coat in the heat-treated condition. (**a**) Backscattered electron image along a cross section of the coating. (**b**) An X-ray diffraction pattern derived from the coating surface; standard patterns of β-NiAl and $PtAl_2$ are also shown. (**c**) An energy dispersive X-ray spectrum showing the elemental composition of the outermost coating layer and the results of quantifying the spectral data

Fig. 7 Analysis of $PtAl_2$ precipitates in the outermost layer of Pt-aluminide bond coat (**a**) Dark-field image of the precipitates formed with the (200) reflection; the inset is a microdiffraction pattern derived from a $PtAl_2$ particle in $\langle 001 \rangle$ orientation. (**b**) Corresponding energy dispersive spectrum showing the elemental composition of the particle

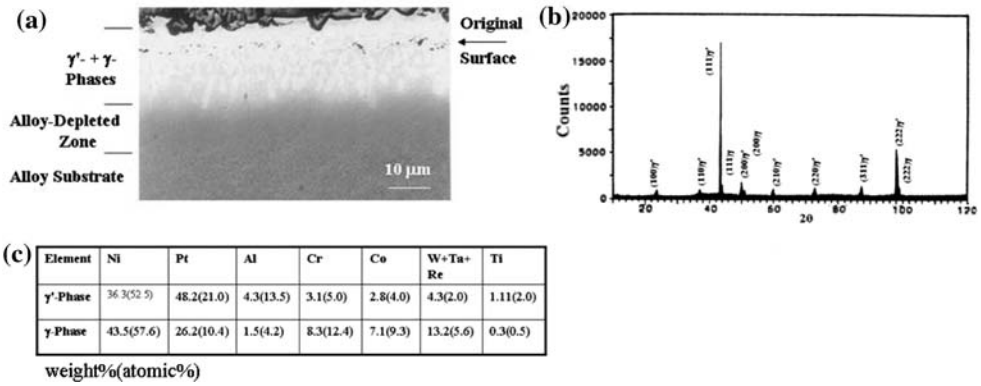

Fig. 8 Characteristic microstructural features of the Pt bond coat in the heat-treated condition. (**a**) Backscattered electron image along a cross section of the coating and into the substrate. (**b**) An X-ray diffraction pattern derived from the surface of the bond coat. (**c**) Chemical compositions of the γ'- and γ-phases near the bond coat surface; wavelength dispersive spectroscopy showed that the only transition metal present in the γ'-phase was Ta

of the γ'- and γ-phases near the surface are shown in Fig. 8c. It is observed that Pt tends to partition to the γ'-phase, which could significantly enhance its diffusional stability [33]. Also, since both Ti and Ta are known to be stabilizers of the γ'-phase, the outer coating layer provided an effective sink for both elements, which could degrade the adherence of Al_2O_3 scale to metallic substrates if present in elemental form [34].

Thermal stability characteristics

Figure 9 shows the effect of exposure time at 1,150 °C on the microstructure of the simple aluminide bond coat. Significant interdiffusion between the bond coat and the alloy substrate after 24 h of exposure was evidenced by the disappearance of the interdiffusion zone and the presence of blocky particles of Ni–Cr–W σ-phase as can be seen by comparing Fig. 9a and b. The coating layer became indistinguishable from the substrate after 48 hours of exposure (Fig. 9c).

In contrast with the simple aluminide, the Pt-aluminide bond coat exhibited a higher thermal stability as shown in Fig. 10. Although the interdiffusion zone continued to grow with exposure time at 1,150 °C, it could be clearly distinguished after 96 h of exposure. However, after 24 h of exposure, the two layers characterizing the bond coat in the heat-treated condition (Fig. 10a) became indistinguishable (Fig. 10b), which could be related to inward diffusion of Pt and outward diffusion of Ni. Associated with this effect was the precipitation of Ni–Cr–W σ-phase. With continued exposure, Ni-rich γ'-phase was formed within the β-phase as shown in Fig. 10c and d.

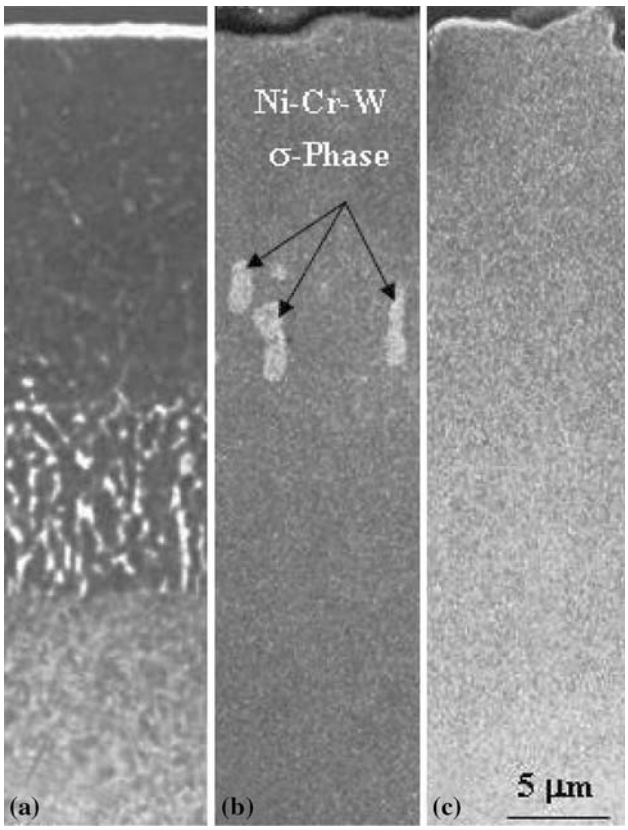

Fig. 9 Backscattered electron images illustrating the effect of exposure time at 1,150 °C on the microstructure of the aluminide coating. (**a**) Heat-treated condition. (**b**) 24 h of exposure. (**c**) 48 h of exposure

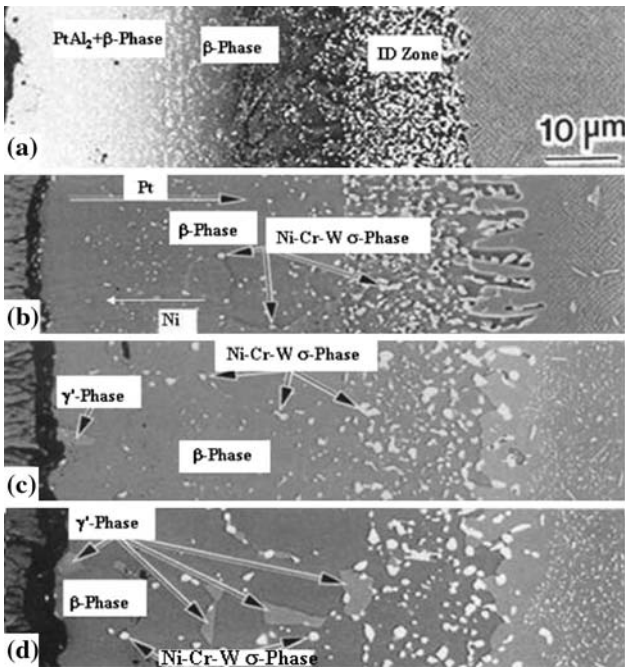

Fig. 10 Backscattered electron images illustrating the effect of exposure time at 1,150 °C on the microstructure of Pt-aluminide coating. (**a**) Heat-treated condition. (b) 24 h of exposure. (c) 48 h of exposure. (d) 72 h of exposure

Figure 11 illustrates the effect of exposure time at 1,150 °C on the microstructure of the Pt bond coat. In comparison with the heat-treated condition (Fig. 11a), the surface layer of the Pt-rich γ'-phase remained rather stable after 96 h of exposure (Fig. 11e). However, considerable inward growth of the inner layer occurred after 24 h (Fig. 11b) resulting in a coarse lamellar structure of γ'-phase, which could be related to interdiffusion. Such a morphology could develop to accommodate the lattice mismatch with the γ-phase resulting from incorporation of refractory transition metals into the γ'-phase. With continued thermal exposure, the γ'-phase became depleted in Pt and as a result releasing both Ta and Ti near the surface, which could eventually degrade the adherence of the surface oxide as shown later.

In agreement with the above results, interdiffusion between the bond coat and alloy substrate expressed as

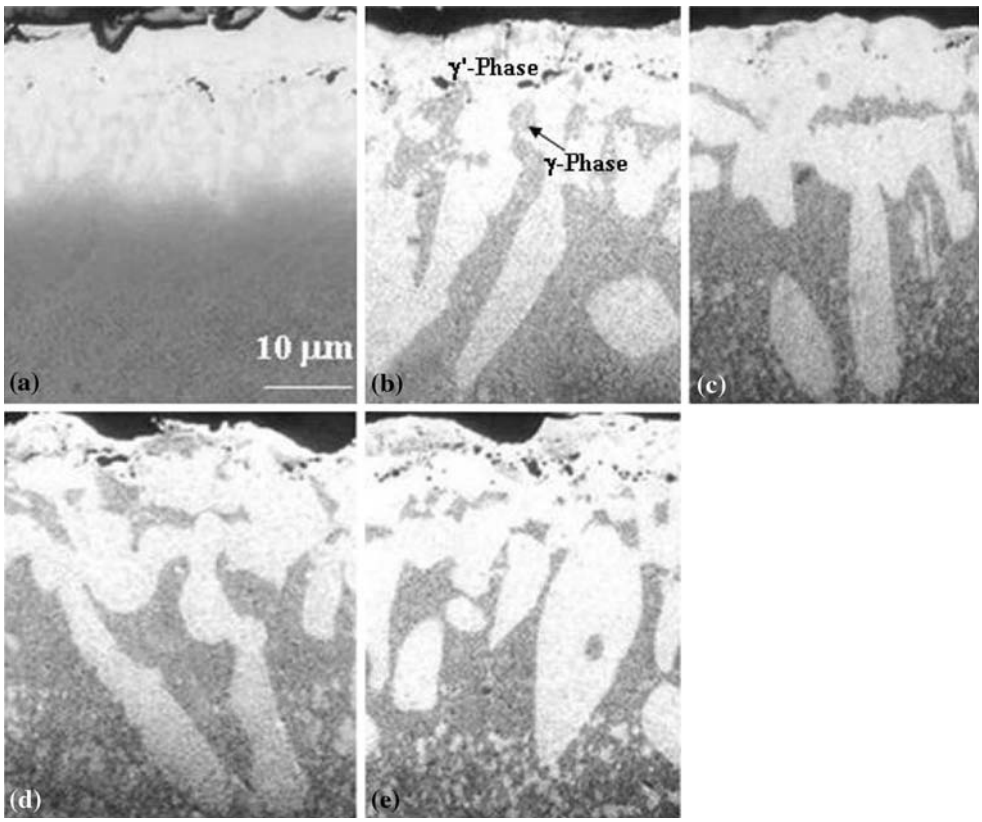

Fig. 11 Backscattered electron images illustrating the effect of exposure time at 1,150 °C on the microstructure of the Pt bond coat. (**a**) Heat-treated condition. (**b**) 24 h of exposure. (**c**) 48 h of exposure. (**d**) 72 h of exposure. (**e**) 96 h of exposure

fractional growth of the coating layer per unit time was found to occur at a slower rate in the Pt bond coat followed by the Pt-aluminide and simple aluminide as shown in Fig. 12. This data was derived from thermal exposure tests at 1,000, 1,050, and 1,100 °C. It is observed that the kinetics of interdiffusion followed a nearly parabolic rate behavior and that the activation energy was nearly the same for the three bond coats (about 290 kJ/mol) suggesting that interdiffusion occurred by the same mechanism. However, since diffusion data related to intermetallic compounds is rather scarce [35], it was

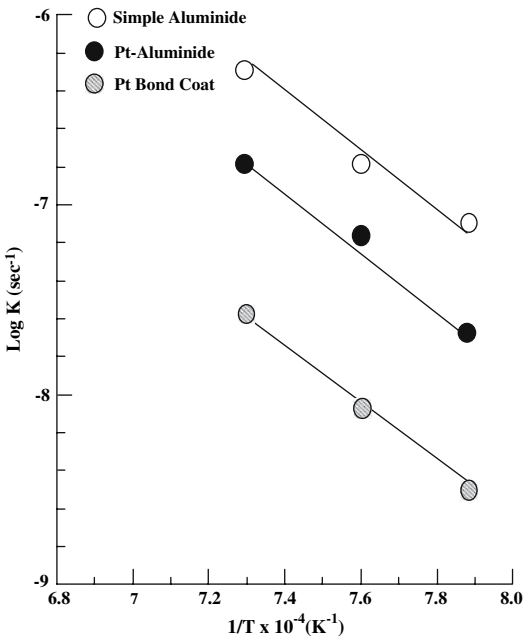

Fig. 12 Effect of temperature (T) on the parabolic rate constant (K) for interdiffusion between the superalloy substrate and various bond coats

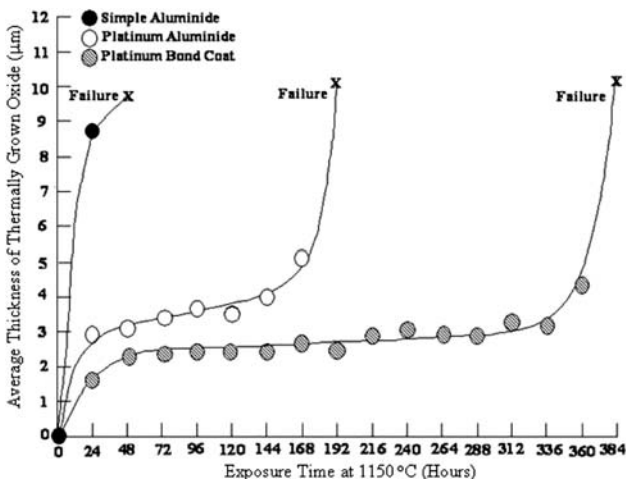

Fig. 13 Thickening rate of thermally grown oxide as a function of exposure time at 1,150 °C for various bond coats

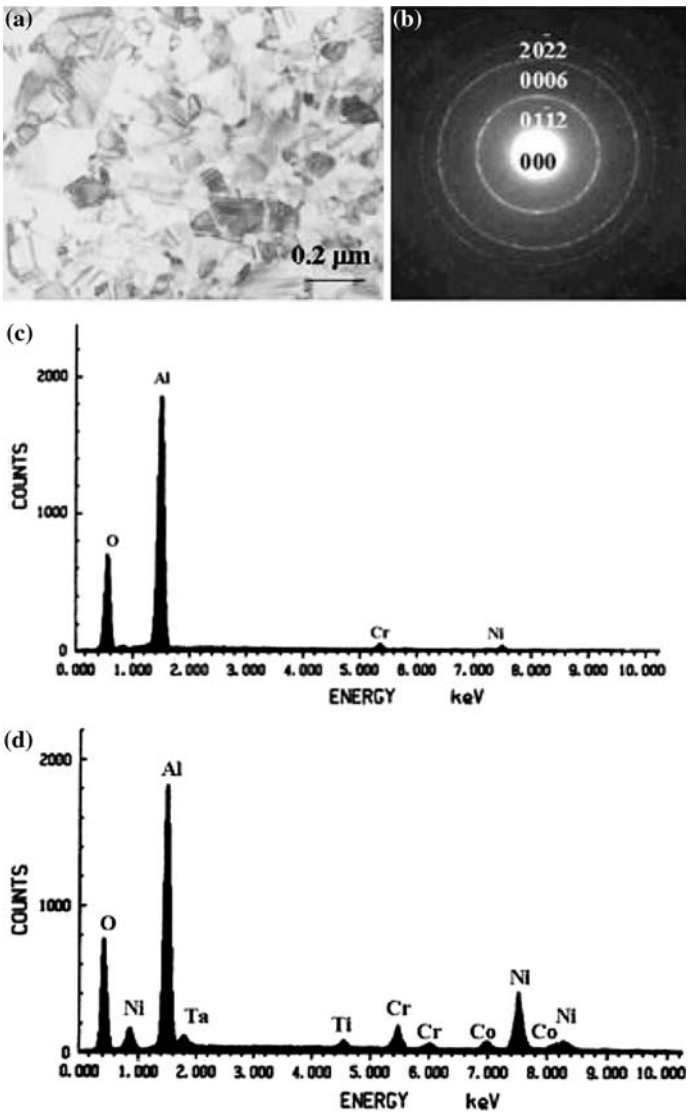

Fig. 14 Analysis of the oxide phase near the oxide-bond coat interface after 96 h of exposure at 1,150 °C. (**a**) Bright-field TEM image showing representative grain structure of the oxide developed by the Pt and Pt-aluminide and bond coats. (**b**) Corresponding selected-area diffraction pattern indexed in terms of the structure of α-Al_2O_3. (**c**) Energy dispersive X-ray spectrum showing the elemental composition of the oxide developed by the Pt bond coat. (**d**) Energy dispersive X-ray spectrum showing the elemental composition of the oxide developed by the Pt-aluminide bond coat

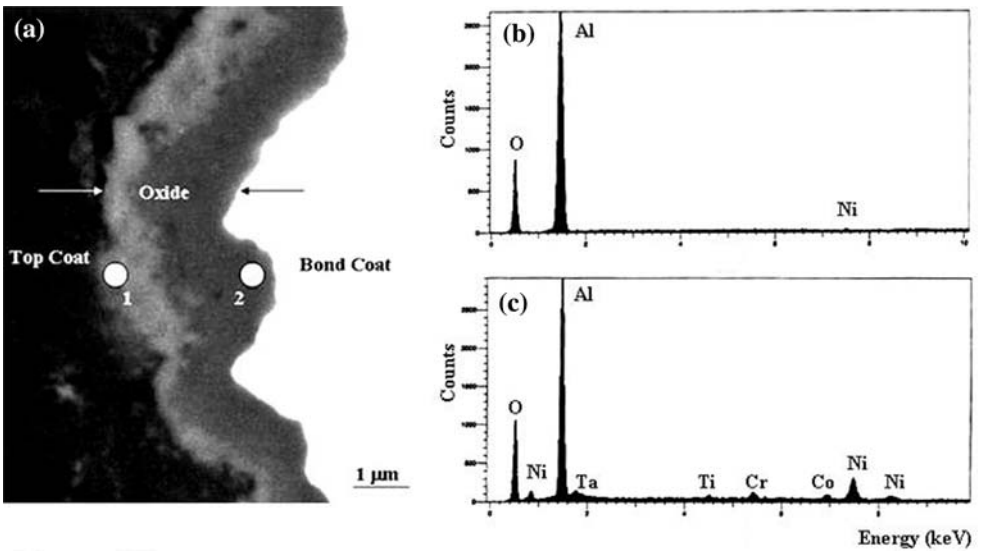

Fig. 15 An example derived from the Pt bond coat to illustrate the composition of the oxide layer after 216 h of exposure at 1,150 °C. (**a**) Backscattered electron image along a cross section of the coating. (**b**) An energy dispersive X-ray spectrum illustrating the elemental composition of the oxide layer near the top coat (region 1 in a). (**c**) An energy dispersive X-ray spectrum illustrating the elemental composition of the oxide layer near the bond coat (region 2 in a)

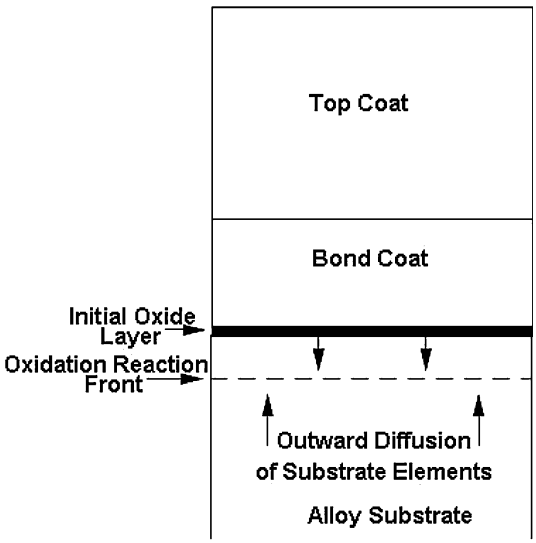

Fig. 16 A scheme illustrating the effect of outward diffusion transport of substrate elements on the dynamics of the oxide-bond coat interface

difficult to correlate the estimated activation energy with a particular diffusion mechanism.

It could be concluded from the above observations that the Pt bond coat had better thermal stability followed by the Pt-aluminide and simple aluminide. This difference in behavior was reflected upon the oxidation properties of the bond coats as demonstrated below.

Oxidation behavior

Figure 13 shows the effect of exposure time at 1,150 °C on the thickness of the thermally grown oxide (total oxide thickness–thickness of initial oxide layer) as measured from SEM images. It is observed that the oxide growth rate was slowest for the Pt bond coat followed by the Pt-aluminide and simple aluminide. This indicated that a one-to-one correspondence existed between thermal stability and oxide growth rate. As an example, Fig. 14 shows the chemical compositions of the oxides developed by the Pt and Pt-aluminide bond coats after 96 h of exposure at 1,150 °C as determined from microchemical analysis of thin foils near the oxide-metal interface. In both cases, the grain structure of the oxide was similar as shown in the bright-field image of Fig. 14a. A corresponding selected-area diffraction pattern characteristic of α-Al_2O_3 is shown in Fig. 14b. As shown in Fig. 14c and d, the Pt bond coat developed a purer scale in comparison with the Pt-aluminide, which could explain at least partially the slower growth rate observed in Fig. 13.

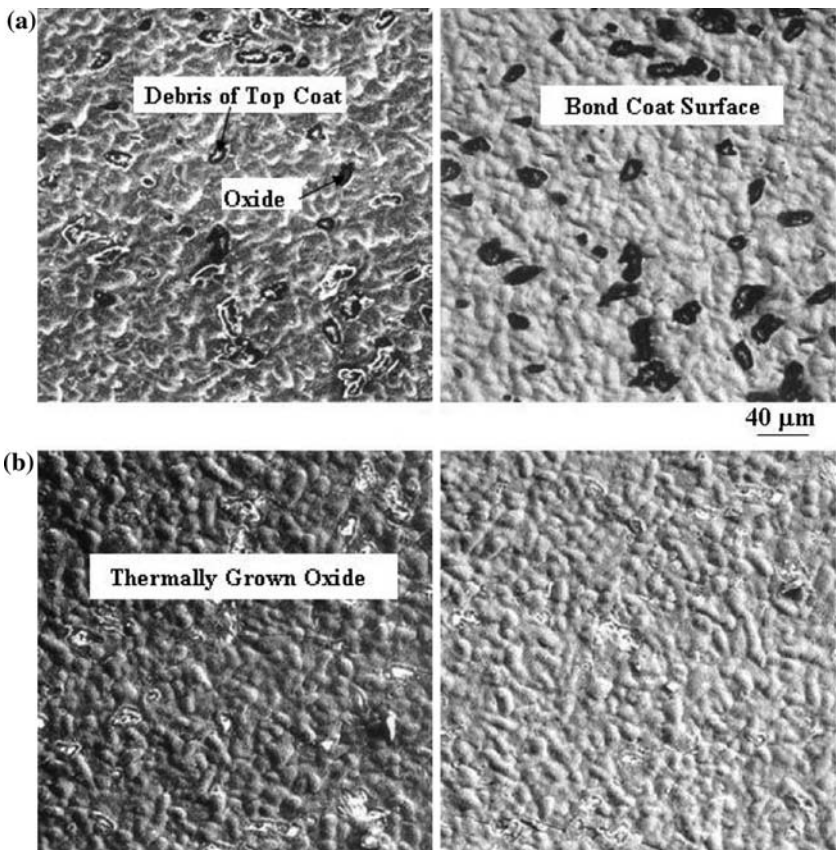

Fig. 17 An example derived from the Pt bond coat to illustrate that spallation of the top coat occurs by decohesion between the thermally grown oxide and bond coat (288 h of exposure at 1,150 °C with a 24-h cycling period to room temperature). (**a**) Secondary electron image (left) and corresponding backscattered image (right) illustrating the bond coat surface. (**b**) Secondary electron image (left) and corresponding backscattered image (right) illustrating the bottom surface of the top coat

In general, after thermal exposure, the oxide near the top coat was found to be relatively pure in comparison with the oxide near the bond coat. An example derived from the Pt bond coat after 216 h of exposure at 1,150 °C is shown in Fig. 15. Similar results were reported earlier for other coating systems [36, 37]. These results indicated that the thermally grown oxide was developed by inward displacement of the interface between the initial oxide layer and bond coat as schematically illustrated in Fig. 16. Therefore, as the interface is displaced inward, the thermally grown oxide becomes contaminated with substrate elements, which diffuse outward.

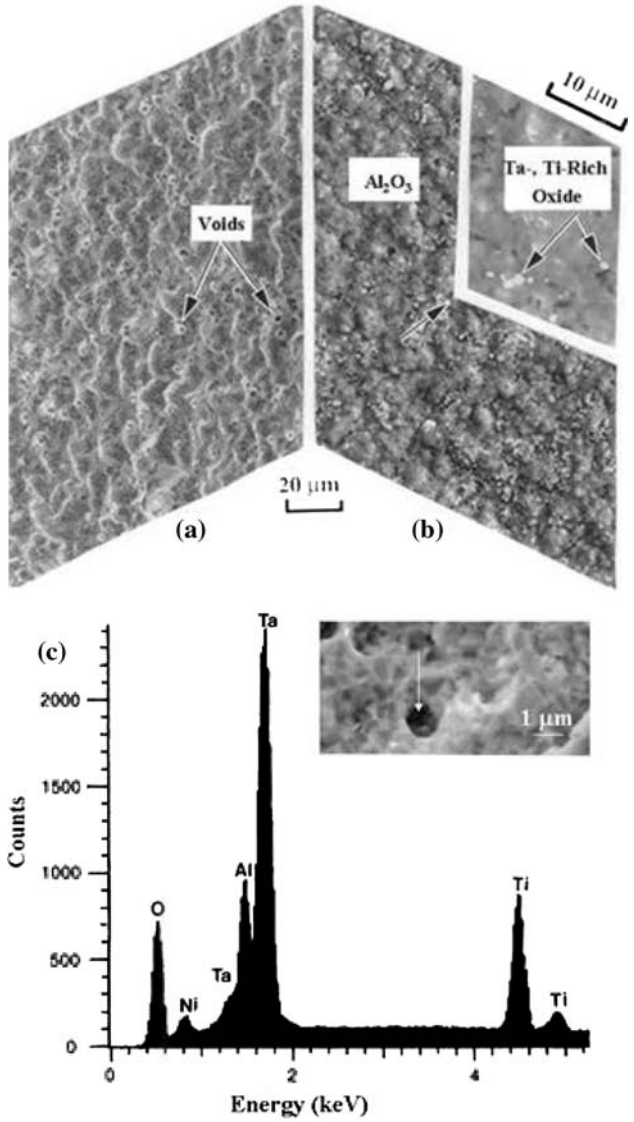

Fig. 18 An example derived from the Pt-aluminide bond coat to illustrate the role of interfacial Ta- and Ti-rich oxide particles in the loss of adhesion between the thermally grown oxide and bond coat (96 h of exposure at 1,150 °C with a 24-h cycling period to room temperature). (**a**) Secondary electron image illustrating the morphology of the bond coat surface, voids are marked by the arrows (**b**) Secondary electron image illustrating the morphology of the bottom surface of top coat covered by the thermally grown oxide containing particles of Ta- and Ti-rich oxides. (**c**) An example illustrating the presence of Ta- and Ti-rich oxide particles at the bottom of voids observed in (**a**)

Failure mechanism

It is evident from the results presented earlier that the performance of a thermal barrier coating system for given top coat, processing parameters, and alloy substrate is critically dependent upon the type of bond coat and its ability to develop and maintain a protective layer of Al_2O_3 scale. As indicated earlier, for all types of bond coats included in this study, spallation of the top coat occurred by decohesion between the thermally grown oxide and underlying bond coat. This is demonstrated in the example of Fig. 17 showing the microstructural features of the surfaces exposed by spallation of the top coat in the system containing the Pt bond coat after 288 h of exposure at 1,150 °C. Similar results were obtained in the case of the Pt-aluminide coating. As shown in the secondary electron image of Fig. 17a, the surface of the bond coat exhibited morphological features similar to those of fracture surfaces produced by microvoid coalescence. However, the surface contained scattered debris of the top coat and some oxide particles as shown in the corresponding backscattered image. In contrast, the bottom surface of the top coat (Fig. 17b) exhibited an inverted morphology and as determined from microchemical analysis, the surface was covered by the thermally grown oxide.

When viewed at higher magnifications, voids at the surface of the bond coat were found to contain particles of Ta- and Ti-rich oxide as illustrated in the example of Fig. 18. As pointed out earlier, both elements were released from the surface layer of the γ'-phase as it continued to lose

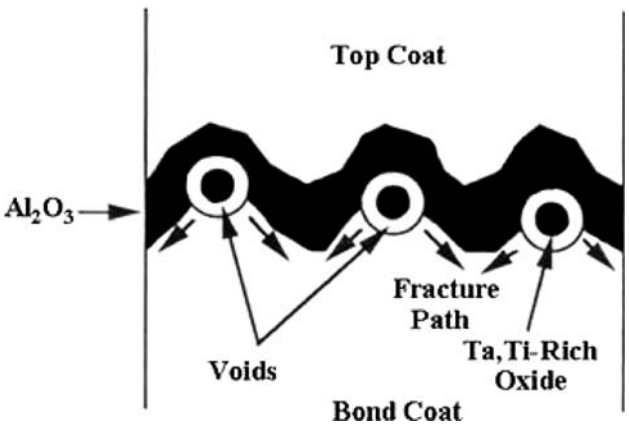

Fig. 19 A scheme illustrating the decohesion of the thermally grown oxide by formation of voids around Ta-, and Ti-rich oxide particles at the oxide-bond coat interface

Pt by interdiffusion with continued thermal exposure. It is recalled that formation of Ta- and Ti-rich oxide particles near the surface is known to degrade the adherence of Al_2O_3 as schematically illustrated in Fig. 19 eventually leading to spallation of the top coat. Since both the Pt-aluminide and Pt bond coats exhibited a qualitatively similar behavior, it could be concluded that Pt decelerates the kinetics of the process leading to spallation of the top coat dependent upon its state of presence.

Conclusions

It is concluded from this study that a significant improvement in the performance of thermal barrier coatings could be achieved by the use of Pt-containing bond coats. Platinum is found to act as a "cleanser" of the oxide-bond coat interface by limiting the transport of elements detrimental to oxidation properties of the bond coat particularly Ti and refractory transition elements. This promotes the formation of purer oxide of a slower growth rate and better adherence to the substrate. However, the exact effect is found to be dependent upon the state of presence of Pt within the outermost layer of the bond coat. Among the bond coats included in this study, a surface layer of Pt-rich γ'-phase is found to produce longer coating life in comparison with a mixture of $PtAl_2$ and β-phase.

References

1. Pomeroy MJ (2005) Mater Des 26(3):223
2. Padture NP, Gell M, Jordan EH (2002) Science 296(5566):280
3. DeMasi-Marcin JT, Gupta DK (1994) Surf Coat Technol 68/69:1
4. Sims CT (1991) Adv Mater Processes 139(6):32
5. Tolpygo V, Clark DR (2005) Surf Coat Technol 200(5–6):1276
6. Tawancy HM, Mohamed AI, Abbas NM, Jones RE, Rickerby DS (2003) J Mater Sci 38:3797
7. Guerre C, Remy L, Molins R (2003) Mater High Temp 20(4):481
8. Yanar NM, Kim G, Hamano S, Pettit FS, Meier GH (2003) Mater High Temp 20(4):495
9. Mumm DR, Evans AG, Spitsberg IT (2001) Acta Mater 49(12):2329
10. Tawancy HM, Sridhar N, Abbas NM, Rickerby DS (2000) J Mater Sci 35:3615
11. Gell M, Vaidyanathan K, Barber B, Cheng J, Jordan E (1999) Metall Mater Trans A Phys Metall Mater Sci 30(2):427
12. Tawancy HM, Sridhar N, Abbas NM, Rickerby DS (1998) J Mater Sci 33:681
13. Dietl U (1994) Surf Coat Technol 68/69:17
14. Sun JH, Chang E, Chao CH, Cheng M (1993) Oxid Met 40(5/6): 465
15. Meier SM, Nissley DM, Sheffler KD, Cruse TA (1992) Trans ASME 114:258
16. Lih W, Chang E, Wu BC, Chao CH (1991) Oxid Met 36(3/4):221
17. Millerc RM (1989) J Eng Gas Turbines Power 111:301
18. Panat R, Hsia KJ, Oldham J (2005) Phil Mag 85(1):45
19. Panat R, Hsia KJ (2004) Proc Royal Soc of London Series A Math Phys Eng Sci 460(2047):1957
20. Tolpygo VK, Clarke DR (2004) Acta Mater 52(17):5115
21. Panat R, Hsia KJ, Cahill DG (2005) J Appl Phys 97(1):art. no. 013521
22. Pint BA (2004) Surf Coat Technol 188:71
23. Tawancy HM, Abbas NM, Rhys-Jones TN (1991) Surf Coat Technol 49:1
24. Schaeffer J, White WE, Vandervoort GF (1989) In: Lang E (ed) The role of active elements in the oxidation behavior of metals and alloys. Elsevier Applied Sciences, London, New York, p 231
25. Jackson MR, Rairden JR (1977) Metall Trans A8:1697
26. Patnaik PC (1989) Mater Manuf Processes 4(1):133
27. Goward GW, Cannon LW (1988) Trans ASME 110(1):150
28. Smith JS, Boone DH (1990) Gas turbine and aeroengine congress and exposition, Brussels, Belgium, June 1990, ASME Paper Ni. 90-GT-319
29. Goodhew PJ (1984) Specimen preparation for transmission electron microscopy. Oxford University Press, Oxford, p 26
30. Goward GW, Boone DH (1971) Oxid Met 3(5):475
31. Goward GW (1970) J Met 22(10):31
32. Wood JH, Goldman EH (1987) In Sims CT, Stoloff NS, Hagel WC (eds) Superalloys II. Wiley Interscience, p 359
33. Giggins CS, Pettit FS (1971) J Electrochem Soc 118:1782
34. Fleetwood MJ (1970) J Inst Met 98:1
35. Hayashi S, Ford SI, Young DJ, Sordelet DJ, Besser MF, Gleeson B (2005) Acta Mater 53(11):3319
36. Levy M, Farrell P, Petit FS (1986) Corrosion 42(12):717
37. Anton DL, Shah DM, Duhl DN, Giamei FA (1989) J Met 41(9):12
38. Lih W, Chang E, Wu BC, Chao CH (1991) Oxid Met 36(3/4):221
39. Wu BC, Chao CH, Chang E (1990) Mater Sci Eng A124:215